

# HYDROGENATION OF GRAPHENE ON Ir(111) BY VIBRATIONALLY EXCITED MOLECULES



AARHUS  
UNIVERSITET

iNANO

Anders Christian Løchte Jørgensen - 201304162  
iNano, Aarhus University

Supervisor:  
Liv Hornekær

Department of Physics and Astronomy, Aarhus University

June 2016

## **Abstract**



# Contents

<b>1</b>	<b>Introduction</b>	<b>1</b>
<b>2</b>	<b>Graphene</b>	<b>2</b>
2.1	Graphene . . . . .	2
2.2	Graphene on Ir(111) . . . . .	3
2.3	Hydrogenation of graphene on Ir(111) using atomic deuterium . . . . .	4
2.3.1	Formation of vibrationally excited Deuterium . . . . .	5
<b>3</b>	<b>Techniques</b>	<b>7</b>
3.1	Scanning Tunneling Microscopy - STM . . . . .	7
3.2	Temperature Programmed Desorption - TPD . . . . .	9
3.3	Low Energy Electron Diffraction - LEED . . . . .	10
<b>4</b>	<b>Experimental Approach</b>	<b>11</b>
4.1	The Coal Chamber . . . . .	11
4.2	STM Imaging and D <sub>2</sub> Dosage . . . . .	12
4.2.1	STM Calibration . . . . .	12
4.2.2	D <sub>2</sub> Dosage . . . . .	13
4.2.3	Sample Annealing and Graphene Repair . . . . .	13
4.3	TPD . . . . .	14
<b>5</b>	<b>Results</b>	<b>17</b>
5.1	Graphene on Ir(111) . . . . .	17
5.2	D <sub>2</sub> on Graphene . . . . .	18
5.2.1	Full Hydrogen Coverage . . . . .	18
5.2.2	1745°C dose . . . . .	20
5.2.3	1593°C dose . . . . .	20
5.2.4	1343°C dose . . . . .	21
5.3	TPD measurements . . . . .	22
5.3.1	Atomic and molecular D <sub>2</sub> - single layered sample . . . . .	22
5.4	Graphene bilayered sample . . . . .	23
5.4.1	TPD of bilayered sample . . . . .	23

5.4.2	STM images of bilayers . . . . .	25
5.4.3	LEED of bilayered sample . . . . .	27
<b>6</b>	<b>Conclusion and future perspectives</b>	<b>29</b>
6.1	conclusion and future perspectives . . . . .	29
<b>A</b>	<b>Additional figures</b>	<b>30</b>
	<b>Bibliography</b>	<b>31</b>

1

# Introduction

# 2

## Graphene

### 2.1 Graphene

Carbon, which not only is one of the key elements in every known life form, also has a wide span of applications ranging from common lead in pencils to jewelry in the form of rare earth diamonds. Extensive research has been conducted on graphene, due to the fascinating abilities of this material such as an electron mobility of  $2.5 \cdot 10^5 \text{ cm}^2 \text{V}^{-1} \text{s}^{-1}$ . [1] which is much greater than the mobility in typical metals of  $50 \text{ cm}^2 \text{V}^{-1} \text{s}^{-1}$ . [2] Furthermore the Youngs modulus of graphene has been measured to 1 TPa and the intrinsic strength of 130 Gpa. [1] A thermal conductivity exceeding  $3,000 \text{ W mK}^{-1}$ , adds to the remarkable abilities of graphene.

Graphene is a two dimensional honeycomb lattice of carbon atoms. Each carbon atom is  $sp^2$  hybridized where one  $s$  orbital and two  $p$  orbitals form three planar bonds with a separation angle of  $120^\circ$ . [3] The distance between the individual carbon atoms is  $1.42 \text{ \AA}$ . Due to the flexibility of the  $sp^2$  bonds in the  $z$  direction, many other structures can be formed by a sheet of graphene, such as fullerenes, carbon nanotubes, and graphite. Fullerenes are the shape of balls, consisting of 60 carbon atoms. These balls are formed from a wrapped up graphene sheet. The graphene sheet is wrapped up due to the formation of pentagons. Carbon nanotubes has the shape of a tube, naturally, and are formed from the

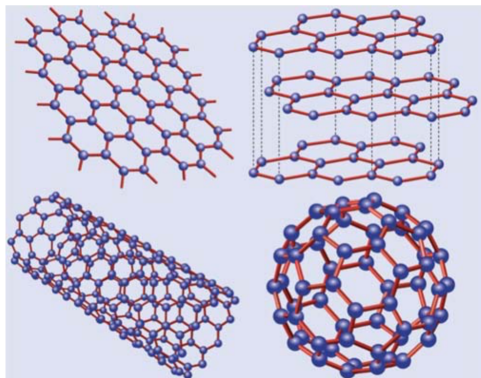


**Figure 2.1:** Graphical interpretation of the different structures of graphene. Top left shows a graphene monolayer beside a 3-layered graphite structure. Bottom left shows a carbon nanotube beside a  $C_{60}$  fullerene.

connection of two edges on a graphene sheet. Graphite, at last, is the structure arising, when multiple layers of graphene are stacked on top of each other. Here the Van Der Waals forces between the individual layers, are the only thing that keeps the layers on top of each other. All of these structures are shown in Figure 2.1. The graphene unit cell consists of only two lattice points, and the lattice vectors can be written as the following:

$$a_1 = \frac{a}{2}(3, -\sqrt{3}) \quad a_2 = \frac{a}{2}(3, \sqrt{3})$$

## 2.2 Graphene on Ir(111)

As a monolayer of graphene is synthesized on top of a metal surface the underlying metal and the graphene monolayer rarely has identical lattice parameters. This causes a mismatch between the two layers which causes areas where the two layers are perfectly aligned as well as areas where both layers are complete out of phase. This causes a phenomenon known as a moiré effect, where a superstructure appears from the two mismatching patterns.

During these experiments, graphene on top of an Ir(111) surface is studied. Ir crystallises as a face centered cubic lattice, and once cut in the [111] direction, the surface atoms have a hexagonal close packed arrangement. [4] The atomic diameter of Ir is 2.715 Å [4], which differs slightly from the graphene lattice with a periodicity of  $2.45 \pm 0.04$  Å [5], and a moiré pattern is therefore expected. Graphene on Ir(111) has a well-defined moiré structure which is depicted in Figure 2.2a. Here the grey atoms show the Ir(111) surface, and the red layer on top corresponds to the graphene sheet. The moiré pattern is seen as bright spots across the surface where an Ir atom is directly below the center of a graphene hexagon. It is seen from Figure 2.2a that the moiré pattern has a periodicity, and the repeat vector is found in the literature with a length of  $25.2 \pm 0.4$  Å.

The graphene on Ir(111) moiré unit cell is outlined in Figure 2.2a and a zoom of this is shown in Figure 2.2b. In this figure the ATOP, FCC and HCP positions are marked by circles. These areas within the unit cell are of special interest due to special alignments between the underlying Ir(111) atoms and the graphene sheet. The ATOP sites are positioned in the corners of the unit cell rhombus where an Ir atom is just below the center of a graphene hexagon. In the HCP site the graphene hexagon is aligned with the two underlying Ir layers as a HCP lattice. This means that an atom from the Ir(S-1) layer is directly under the center of a graphene hexagon. In the FCC site, an atom from the Ir(S-2) layer is directly under the center of a graphene hexagon. Every second carbon atom is directly above an Ir atom, in both the HCP and FCC site.

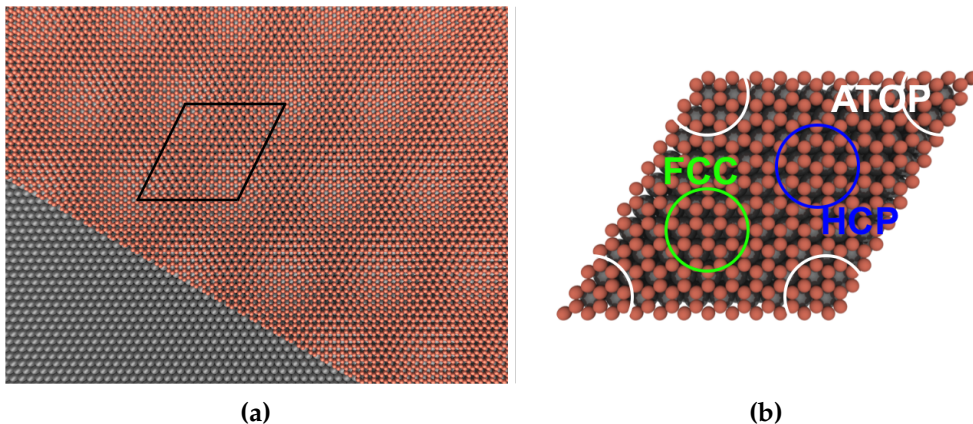


**Figure 2.2:** Graphical interpretation of graphene on Ir(111). (a) shows a Ir(111) (grey) surface with the moiré structure once the graphene sheet (red) is on top. (b) shows a moiré unit cell. [6]

## 2.3 Hydrogenation of graphene on Ir(111) using atomic deuterium

The properties of graphene changes drastically with chemical functionalization of different species. The adsorption of any species is highly determined by the underlying surface, which in this study is Ir(111). The adsorption of hydrogen to the Gr/Ir surface is a highly wanted mechanism to understand, due to the special abilities arising from the functionalization of graphene by hydrogen. These effects include a bandgap opening of at least 450meV. [7] The bandgap opens up for a large number of possibilities for the usage of functionalized graphene, where the most appealing is constructing a new type of field effect transistors. Other forms of applications of functionalized graphene is within energy storage. Due to the one atom thick monolayer it is desirable to use graphene to store hydrogen.

As hydrogen is adsorbed to the graphene monolayer, the structural arrangement is changed. Due to the adsorbed hydrogen atom, the graphene undergoes a transition from  $sp^2$  hybridization to  $sp^3$  hybridization. This implies that the otherwise flat graphene sheet is distorted due to the 3-dimensional conformation of the bonds in the  $sp^3$  hybridization. Every second carbon atom is turning downwards and constructs a bond to the underlying Ir(111) surface. This is only possible in the HCP and FCC sites of the moiré unit cell where every second carbon atom of the graphene is directly above an Iridium atom. This induce that the hydrogenation of graphene follows the moiré pattern. [8] It is therefore expected to observe a superstructure from the hydrogenated surface with the same periodicity as the moiré pattern.

A graphical interpretation of the hydrogenation of graphene on Ir(111) is shown in figure 2.3, which is made by Line Kyhl. Here it is seen that clusters of hydrogen bind to the carbon atoms in the FCC and HCP sites. Figure 2.3b demonstrates how every other carbon atom binds to the Ir(111) surface and every other binds to a hydrogen atom. Furthermore dimers of hydrogen is seen binding to the surface at the ATOP sites. In these regions the distance to the Iridium is increased compared to the FCC and HCP sites. In these areas the graphene resemble free standing sheets and no bonds are formed between the Iridium and the carbon atoms.

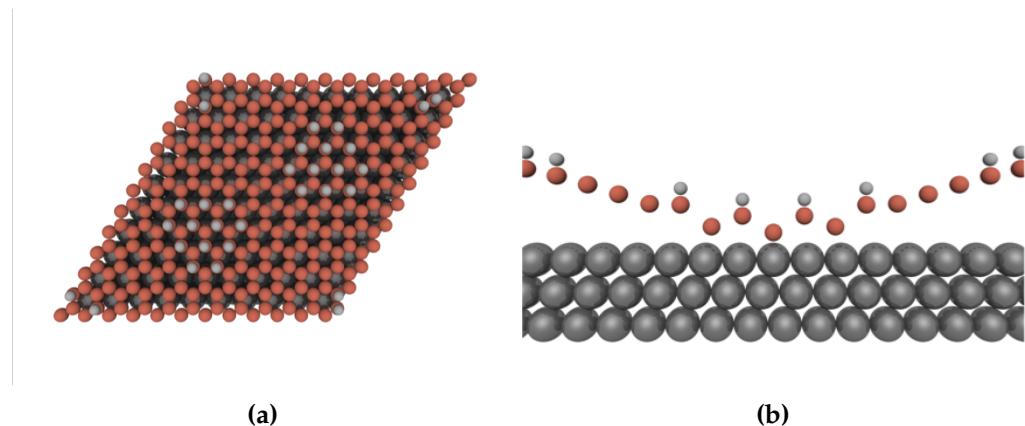


**Figure 2.3:** Graphical interpretation of the hydrogenation of graphene on Ir(111) by hot atoms. [6]

### 2.3.1 Formation of vibrationally excited deuterium

Vibrationally excited hydrogen molecules have been found to arise from recombinative desorption from metal walls. This happens as atomic hydrogen from a gas phase recombine with hydrogen stuck to the surface. This mechanism produces excited molecules at vibrational states as high as  $v'' = 9$ . [9] The vibrational states follow a boltzmann distribution at levels up to  $v'' = 3$ , and a non boltzmann distribution with an excess off excited states at higher levels. The energy of a hydrogen molecule in the  $v'' = 9$  state is 3.56 eV, which is enough to dissociate onto free standing graphene with an adsorption barrier ranging from 3.3 eV to 3.9 eV for relaxed graphene, and ranging from 4.3 eV to 4.7 eV for unrelaxed graphene. [10]

The formation of vibrationally excited molecules is limited by the amount of atomic hydrogen produced. By using a hot filament, it is possible to dissociate hydrogen molecules on the filament surface, and thereby create an atomic gas phase. The coverage on this filament is low once heated and the fraction of a monolayer is in the order of  $\theta < 10^{-4}$ . [11] Therefore a valid assumption is that the hydrogen molecules from the gas phase are impinging on a clean surface. From this assumption the flux of atomic hydrogen from the surface is given by: [11]

$$\phi(H) = 2s_m P_a \phi(H_2) \quad (2.1)$$

Here  $s_m$  is the sticking probability of molecular hydrogen and  $P_a$  is the atomization probability.  $\phi(H_2)$  is the flux of molecular hydrogen towards the surface. The factor of 2 accounts for the two hydrogen atoms resulting from the dissociation of a single molecule. The sticking probability is a material and temperature dependant factor, and the flux of molecules towards the surface is a function of the pressure of the gas phase. The probability of atomization is given by the following: [11]

$$P_a = \frac{1}{4} [ \{ (K_p/\gamma p)(K_p/\gamma p + 8) \}^{\frac{1}{2}} - K_p/\gamma p ], \quad (2.2)$$

### 2.3. Hydrogenation of graphene on Ir(111) using atomic deuterium

---

where  $K_p$  is the equilibrium constant of the atomization reaction,  $\gamma = \sqrt{\frac{T_f}{T_g}}$ , with subscripts indicating the temperature of the filament and gas respectively. The gas pressure is  $p$ . During this study the hydrogenation of graphene on Ir(111) is investigated, and the hydrogenation threshold is estimated. By changing the amount of atomic hydrogen impinging the walls in the UHV chamber, the point at which no hydrogen is adsorbed to the graphene on Ir(111) surface can be found. During these experiments the gas pressure as well as the gas temperature is kept constant. Hence the temperature of the hydrogen cracker is altered in order to find the temperature, at which the number of excited molecules, in the high vibrational levels, is close to zero.

# 3

## Techniques

### 3.1 Scanning Tunneling Microscopy - STM

The main technique used in this study is scanning tunneling microscopy (STM), and more specifically the Aarhus STM. The Aarhus STM is an enhancement of the original version invented by Heinrich Rohrer and Gerhard Binnig in 1981. [12] The STM is used to create surface images with atomic resolution of conducting samples, which makes the technique irreplaceable in this study.

Images of the sample surface are made from scanning the sample surface with a very sharp metal tip. As the sample is scanned, the tunneling current between the tip and the sample is mapped, in order to create a topographical image of the surface. The high sensitivity of the STM stems from the tunneling transmittivity which depends exponentially on the distance between the tip and the sample. The distance to the surface is measured indirectly by the tunneling current which changes by about a factor of 10 for every ångstrøm. [13] A figure of the aarhus STM is shown in figure 3.1. The sample (1) is positioned within the Tantalum sample holder (2) and both are held tight by clamps (3). The STM tip held by a macor holder (5) is seen just above the sample (4) and this is controlled by the piezo scanner tube (6). In continuation of the scanner tube, a rod (7) is mounted which extends through another configuration of piezo elements abbreviated "The inchworm". This inchworm motor, held by another macor ring (8), is able to clamp to the rod and either expand or contract, in order to approach and retire the tip from the sample. The STM is thermally isolated from the rest of the environment by quartz balls (10). If the temperature drops during cooling despite the thermal isolation, a zener diode (11) is mounted in order to heat the STM.

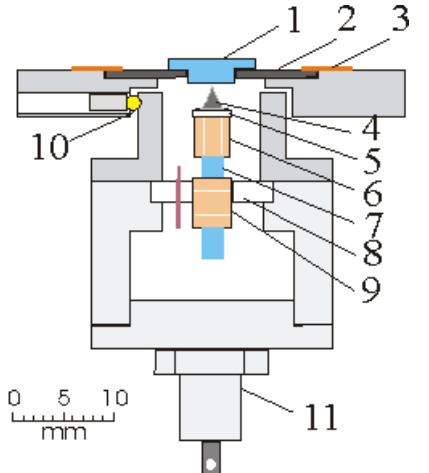


**Figure 3.1:** Schematic of the aarhus STM. [12]

At relatively large distances the vacuum barrier that the electrons perceive is too high, and no tunneling occurs. As the distance between the sample and the tip is reduced the probability of an electron tunneling through the vacuum barrier increases until a certain point where tunneling happens. In order to achieve tunneling, the electrons need an energy at least equal to the work function given by;  $\phi = E_{vac} - E_F$ , where  $E_{vac}$  is equal to the energy of the vacuum barrier and  $E_F$  is the energy at the fermi level. To keep a current flowing a bias is applied between the sample and the tip. The energy of the fermi levels are altered by  $eV$ , where  $V$  is the voltage difference. This voltage difference establishes a constant flowing tunneling current, which can be calculated using the Wentzel-Kramers-Brillouin approximation. The tunneling current is given by: [14]

$$I = \int_0^{eV} \rho_s(E, r) \rho_t(E - eV, r) T(E, eV, r) dE, \quad (3.1)$$

where  $\rho_s(E, r)$  and  $\rho_t(E - eV, r)$  are the local densities of states (LDOS) at energy  $E$  at the position  $r$ .  $T(E, eV, r)$  is the tunneling transmission probability, for electrons with energy  $E$  and an applied voltage of  $eV$ . When the applied voltage,  $eV < 0$ , the sample is negatively biased, and when  $eV > 0$  the sample is positively biased.

The tunneling transmission probability is given by the following: [14]

$$T(E, eV) = \exp \left( -\frac{2Z\sqrt{2m}}{\hbar} \sqrt{\frac{\phi_s + \phi_t}{2} + \frac{eV}{2} - E} \right), \quad (3.2)$$

where  $Z$  is the distance between the sample and the tip, and  $m$  is the mass of the electron.  $\phi_s$  and  $\phi_t$  are the workfunctions of the sample and the tip respectively. From this expression it is seen that once the sample is negatively biased, the limits in the integral range from 0 to  $eV < 0$ . Equation 3.2 then returns the highest probability at  $E = 0$ , which is the energy at the fermi level of the sample. In contradiction, at a positive sample bias, equation has the limits 0 to  $eV > 0$ . Now equation 3.2 returns the highest probability at the energy  $E = eV$ , which is the energy at the fermi level of the tip. This means the negatively biased electrode always has the highest tunneling transmission probability, and the electrons always flow from this to the positively biased electrode. The tunneling current can be calculated, assuming that the density of states of the sample and the tip are constant and that  $eV \ll \phi_{s,t}$ . [14, 15]

$$I = \rho_s \rho_t V \exp \left( -\frac{2\sqrt{2(\phi_s + \phi_t)m}}{\hbar} Z \right). \quad (3.3)$$

From this it is seen that the tunneling current, as mentioned, depends exponentially on the distance to the sample. Furthermore it is seen that the tunneling current depends on the applied bias, the LDOS of the sample and the tip, and their respective workfunctions.

## 3.2 Temperature Programmed Desorption - TPD

The desorption kinetics of hydrogen from the graphene on Ir(111) surface is studied by temperature programmed desorption (TPD). Here the temperature of the sample is raised as a function of time. The temperature program,  $\beta(t) = \frac{dT}{dt}$ , is commonly a linear ramp with a rate ranging from  $10^{-1}$  to  $10^2$  K s $^{-1}$ . [16] The adsorption versus desorption rate is studied by monitoring the time evolution of the coverage of the sample denoted  $\theta$ . The coverage of a given adsorbate is given as the number of adsorbates on the surface as a percentage of the number of adsorbate sites. The time evolution of the coverage is naturally given by the rate of adsorption,  $R_a$ , subtracted by the rate of desorption,  $R_d$ .  $R_a$  and  $R_d$  is given by: [16]

$$R_a = \frac{S(\theta, T) P a_s}{\sqrt{2\pi m k_B T}} \quad R_d = r_d(\theta, T) \theta^n \quad (3.4)$$

For  $R_a$ ; the initial factor  $S(\Theta, T)$  is the sticking factor, which is a substrate dependant function describing the probability of an adsorbate to stick to the surface. The second factor describes the flux of atoms impinging the surface, and this expression is known as the Hertz-Knudsen equation.  $R_d$  is described as a rate of desorption multiplied by  $\theta^n$ , where  $n$  is the desorption order. Common desorption orders are,  $n = 1$  describing molecular desorption, or  $n = 2$  describing associative desorption where species recombine on the surface as they desorb. During these experiments it is assumed that hydrogen adsorbed to graphene on Ir(111) has a first order desorption rate.

When conducting the TPD measurement the adsorbates desorb from the surface at a certain rate, until the surface is clean. The desorbed molecules are analysed by a quadropole mass analyzer. A typical evolution of the coverage and rate of desorption is seen in Figure 3.2 as well as a typical TPD curve measured by the quadropole. Here it is seen that the rate of desorption, in theory, rise exponentially with the temperature. In practice, however, the counts of desorbed molecules eventually fall off to zero, as the surface coverage approach zero. The number of desorbed molecules can be described by the Polanyi-Wigner equation, which is given by: [16, 18]

$$I(T) \sim -\frac{d\theta}{dt} = v(\theta, T) \cdot \theta^n \cdot \exp\left(\frac{-E_{des}(\theta, T)}{k_B T}\right), \quad (3.5)$$

Where  $I(T)$  is the number of molecules and  $v(\theta, T)$  abbreviated the exponential pre factor. A simple and applicable approach to TPD spectra has been proposed by Redhead from which the desorption energy can be calculated. [16] It is assumed that a first order desorption from the surface is happening. Furthermore the exponential pre factor as well as the desorption energy is assumed to be coverage independent. The energy of desorption is then approximated by the following: [19]

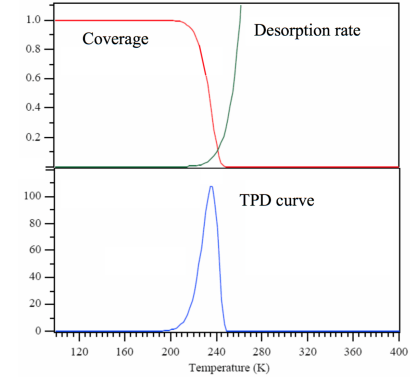


Figure 3.2: [17]

$$E_{des} \approx RT_P \left[ \frac{vT_P}{\beta} - 3.64 \right] \quad (3.6)$$

This equation is used to estimate the energy of desorption from the TPD measurements. A common exponential prefactor of  $v = 10^{13}s^{-1}$  is used. This factor might, however, vary between  $10^{10}s^{-1}$  to  $10^{20}s^{-1}$  [16]. This results in a significant error from the calculated energy of desorption of  $\pm 20\%$ .

### 3.3 Low Energy Electron Diffraction - LEED

# 4

# Experimental Approach

## 4.1 The Coal Chamber

The experiments are carried out under UHV (ultra high vacuum) conditions, with pressures lower than  $1 \cdot 10^{-9}$ mbar. This is crucial because contaminants adsorb to the surface which ruins the quality of the data. The minimal amount of time needed to create a monolayer of contaminants on the surface can be calculated by the Hertz-Knudsen equation mentioned in chapter 3. It is assumed that the sticking coefficient is equal to 1, and that a monolayer require  $10^{15}$  atoms pr.  $\text{cm}^2$ . [20] Taking  $10^{15}$  and dividing by the rate of impinging molecules on  $1 \text{ cm}^2$  at 300K, given by the Hertz-Knudsen equation, it is found that the contamination time is inversely proportional to the pressure. A mass of 4 amu has been used as the mass of the impinging molecules.

$$t_{def} = \frac{10^{15} \text{ atoms/cm}^2 \cdot \sqrt{2\pi m k_B T}}{P a_s} \quad t_{def}(1 \cdot 10^{-6} \text{ mbar}) \approx 13 \text{ s} \quad t_{def}(1 \cdot 10^{-9} \text{ mbar}) \approx 219 \text{ min} \quad (4.1)$$

By inserting a pressure of  $1 \cdot 10^{-6}$ mbar it is found that the surface is completely covered with contaminants within seconds. However at a pressure of  $1 \cdot 10^{-9}$ mbar it will take hours to completely cover the surface.

During this project the UHV chamber named 'The Coal Chamber' is used, which is one of many vacuum chambers in the Surface Dynamics lab. The equipment used in this study mounted on The Coal Chamber, is described in the following section along with the experimental approach. The sample consists of a circular disk of Iridium cut in the (111) direction. This disk is placed in a circular hole in the middle of a flat square sample holder made of Tantalum. A cutout is present in the top of the sample holder. This is grabbed by a transfer arm and a wobble stick, in order to manoeuvre the sample within the UHV chamber. In the lower end of the sample holder a K-type thermocouple plug is mounted. Chromel and alumel wires are attached to their respective connectors on the plug, and the two wires are spot welded. The wires are placed in the middle

of the sample holder, right above the Ir crystal, such that the temperature of the sample can be measured. At last, the Ir crystal is kept in place by spot welding two tantalum strips across the crystal and thermocouple, on the backside of the sample holder.

The sample is introduced to the coal chamber from a loadlock where it is attached to a transfer arm. Transfer of the sample from the loadlock to the main chamber takes place as the pressure in the loadlock is reduced to about  $5 \cdot 10^{-7}$  mbar by a turbo pump. Once the pressure is low, a valve is opened between the loadlock and the main chamber. By using the transfer arm, the sample is directed into the manipulator in the center of the main chamber. From here the sample can be transferred to the STM or annealed by a filament residing in the manipulator.

## 4.2 STM Imaging and D<sub>2</sub> Dosage

The STM was used to get a visualization of the coverage of hydrogen on the sample surface, and to analyse the sample between the different experiments. The STM within 'The Coal Chamber' is an Aarhus STM which is described in chapter 3. Two modes can be used during operation. These modes are the constant current and the constant height mode. In the constant current mode, the tip has a dynamic z-distance to the sample in order to keep the tunneling current constant. This means that the tip moves closer to the sample at areas with a low LDOS and further away from the sample at high LDOS. The current is kept constant by a feedback loop, and the change in height is mapped as the data. The tip height is fixed during constant height mode, in contradiction to the constant current mode. As the tip scans the surface, the tunneling current changes since the distance to the sample varies. Therefore the topography of the surface is mapped as the tunneling current. Since no feedback loop is required, and the tip height is fixed, the time required to create an image is lower in constant height mode. The tip is, however, much more likely to crash into defects on the surface, since no feedback loop is used. The advantages of the constant current mode include higher image quality, and a lower probability of damaging the tip. This scanning mode is therefore used during the experiments.

### 4.2.1 STM Calibration

the tip of the STM is moved by the piezoelectric scanner tube, as mentioned in chapter 3. This is highly sensitive to temperature fluctuations and chamber conditions. Therefore a calibration is needed in order to ensure that the STM images are in the correct sizes. The STM is calibrated using images with atomic resolution. Figure 5.1c, from the results in chapter 5, shows the image used for calibration which is of pure graphene on Ir(111). The length of ten graphene hexagons were measured in the x- and y-direction, and the calibration parameters were found by correcting the measured value to match the length of ten graphene hexagons found in the literature. This results in calibration parameters of:

$$X : 1.000, \quad Y : 1.033 \quad (4.2)$$

These calibration parameters were used on all STM images shown in chapter 5. A single calibration used on all images should be all right, since all the STM images were gathered within the same

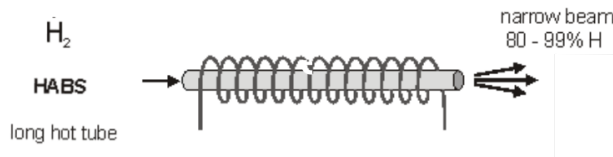


Figure 4.1

chamber baking.

#### 4.2.2 D<sub>2</sub> Dosage

As described in chapter 2, the production of atomic hydrogen, is a necessity in order to achieve vibrationally excited atoms. Therefore a hydrogen atom beam source was used (from now on 'the doser'), in order to dissociate D<sub>2</sub> molecules. The doser consists of a tungsten capillary capable of reaching temperatures up to 2100 °C. [21] The capillary is heated by a tungsten filament surrounding the outside, as seen in Figure ???. The temperature of the doser is measured with an integrated C-type thermocouple.

Each time the graphene on Ir(111) sample was dosed with excited molecules the sample was facing away from the doser. Furthermore the built in shutter of the doser was closed. By doing so, no atomic hydrogen reached the sample surface. During dosages of vibrationally excited molecules the ion gauge was turned off. The ion gauge ionizes the molecules within the chamber, and a dissociative attachment process happens once D<sub>2</sub> receives an electron. This results in a formation of atomic hydrogen. [9] The ion gauge is therefore a source of atomic hydrogen as well as the hot doser, which is why it was switched off. The pressure within the chamber could not be measured during doses, and therefore the chamber pressure estimated from the backing pressure. A pirani gauge was attached to the gasline between the hydrogen source and the doser. A calibration, of the pressure measured with the pirani gauge compared to the chamber pressure, was done with the ion gauge turned on. The aim was a chamber pressure of  $5 \cdot 10^{-7}$  mbar. The calibration measurement gave the following pressures:

$$\text{chamber pressure : } 5.11 \cdot 10^{-7} \text{ mbar} \quad \text{pirani pressure : } 6.7 \cdot 10^{-2} \text{ mbar} \quad (4.3)$$

During the hydrogenation of graphene on Ir(111) with atomic hydrogen, the sample was positioned right in front of the tungsten capillary with an open shutter. The ion gauge was turned on during these doses, since the aim was a completely hydrogenated graphene on Ir(111) surface.

#### 4.2.3 Sample Annealing and Graphene Repair

The surface of the sample is kept clean by annealing to high temperatures by the filament in the manipulator. This ensures that contaminants on the surface are removed, in order to raise the quality of the STM images. After each dose of D<sub>2</sub> the sample was scanned by the STM. Hereafter the hydrogen, adsorbed on the surface, was removed by heating the sample above 900K. The graphene on the sample was checked, after cleaning the surface, in order to ensure that the number

of defects was at a minimum. The size and shape of these are discussed in chapter 5. If too many defects were present, the graphene on the sample was repaired by chemical vapour deposition (CVD), if a large number of defects were present on the surface. The sample was heated above 900°C in an ethylene pressure in the range of  $1 \cdot 10^{-6}$  mbar. CVD growth of graphene is possible at temperatures above 1120 K, and the structural quality increases with the temperature. [22] During CVD the temperature of the sample surface was measured by an optical pyrometer, since the thermocouple measures the temperature on the backside of the Ir crystal. It is crucial that the Ir(111) surface is at least 1120K in order to break the ethylene bonds on the Ir(111) surface. As a further study of the dissociation of hydrogen on graphene, bilayered graphene were grown on the Ir(111) surface. This was done according to the CVD procedure explained above. However, the sample was annealed for a long time (1-2 hours) during the growth of bilayers.

### 4.3 TPD

A quadrupole mass analyser is connected to the UHV chamber, and this was used to investigate the desorption of deuterium from the sample surface. The sample was positioned in the manipulator and heated by the filament as the experiments were carried out. From here the nozzle of the mass spec was brought within millimeters of the sample. The temperature was logged together with the amount of deuterium detected by the quadrupole. The mass spec was set to count masses of 4 amu, in order to exclude other molecules than deuterium. This setup was made with the computer program 'MASsoft' by Hiden Analytical.

A Eurotherm 2704 controller was used to control the current running through the filament in the manipulator. The controller was programmed to ramp the sample temperature from 300K to 900K at a rate of 1K per second. At maximum temperature the eurotherm was set to rest for 30s, and then slowly decrease current as the temperature dropped to a final temperature of 300K. This cycle was performed each time a TPD measurement was carried out. After this procedure all of the deuterium on the surface is desorbed from the sample.

As mentioned the temperature measured by the thermocouple is only valid for the backside of the sample. Therefore a calibration of the system is needed in order to find the correct peak temperatures. A calibration was done where the sample surface was measured with an optical pyrometer along with the thermocouple temperatures. Both temperatures were logged each time the temperature rose 30°C. The results from this calibration are seen in Figure 4.2. It is seen that there is no linear temperature ramp until the thermocouple reading is around 600K. This is due to the limitations of the pyrometer. The pyrometer measures the emitted radiation from a solid object, and in order to get a reading, the intensity of the emitted light from the measured object must be significant. [23] However, a fit was made from the data points with a linear tendency. The fitted line had the following parameters:

$$T_{surface} = T_{TC} * 0.7921 + 131.2$$

In figure 4.3a the data obtained from a typical TPD measurement is shown. Since the desorption of D<sub>2</sub> from the surface is investigated, a mass of 4 amu is monitored along with the temperature of

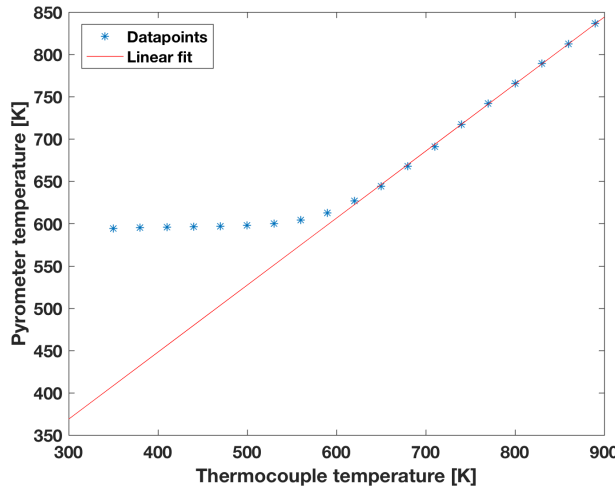


**Figure 4.2:** Calibration of the temperature during the TPD measurements. The temperature of the surface measured by an optical pyrometer is plotted against the thermocouple temperature.

the sample. It is seen that the temperature follows a linear ramp. Some fluctuations are however seen in the beginning and end of the temperature interval. These measurements were carried out on the main graphene on Ir(111) sample.

During the last period of the project a new sample of graphene on Ir(111) was used to conduct TPD measurements. This sample had a freshly made monolayer of graphene. This sample also had a thermocouple which seemed to have a loose connection, which caused problems with the temperature ramp. The readings from this thermocouple dropped out at some points, and generally seemed unstable. Furthermore, since the thermocouple was changed and a new sample holder was used, the Eurotherm controller parameters needed to be autotuned, in order to achieve a linear temperature ramp once again. This autotuning was unsuccessful, and the results from one of the TPD measurements from this sample can be seen in figure 4.4. It is seen on figure 4.4a that the temperature ramp far from linear. The jumps in temperature do not seem to be systematic, which might indicate that the thermocouple as well as the controller parameters both had influence on the bad temperature ramp. The influence of the non linear ramp is also seen on the D<sub>2</sub> counts, where small peaks appear when the temperature changes rapidly. As seen on figure 4.4b another peak appears right after the initial peak due to the jump in temperature. The initial peak was judged to fit the desorption of hydrogen best, and hence this peak value was used, as seen from the green circle in the figure.

Peak values were found by fitting a triple gaussian function to the data points around the peak. The initial peak value was estimated by visual observation, and the data points within  $\pm 60^\circ\text{C}$  are included in the fit. The temperatures at the maxima of the fits were determined, and these values are presented in chapter 5 as the peak temperatures. An example of the fit to the data points is shown in figure 4.3b. From this figure it is seen that the temperature at which the maximum counts number of counts are observed, not necessarily corresponds to the correct peak temperature. The green circle in figure 4.3b shows the found peak from which the sample temperature was gathered.

These temperatures are found for each TPD measurement, and the desorption energy is estimated by the Redhead method described in chapter 2.

In order to compare the individual peaks, the background was subtracted from every datapoint. The sample was positioned stationary in front of the nozzle and data was acquired for a period of time before each temperature ramp was started. These data points prior to the temperature ramp were used to calculate a mean background count, which was subtracted.

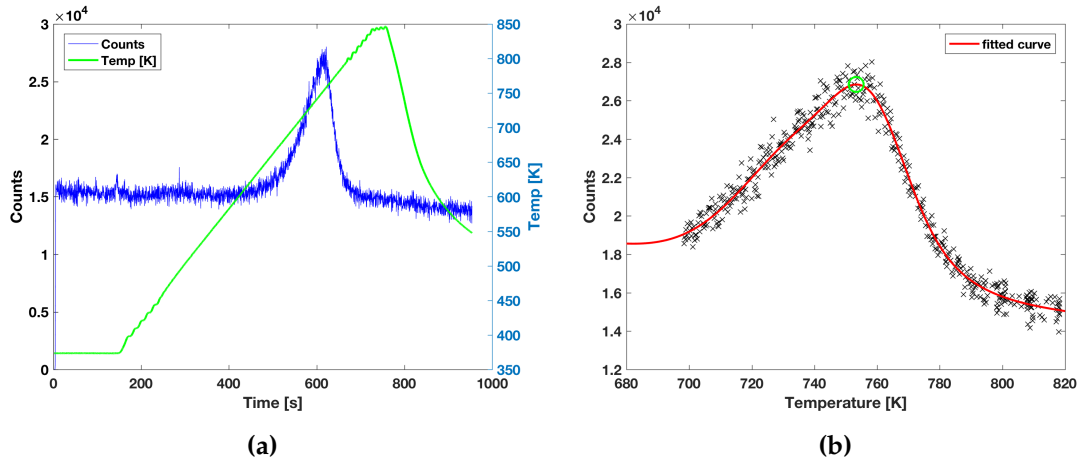


**Figure 4.3:** example of TPD measurements from the main sample. (a) shows data acquired from the quadrupole mass analyser and thermocouple readings. (b) shows the fitted curve to the datapoints within  $\pm 60^\circ\text{C}$  of the estimated peak value.

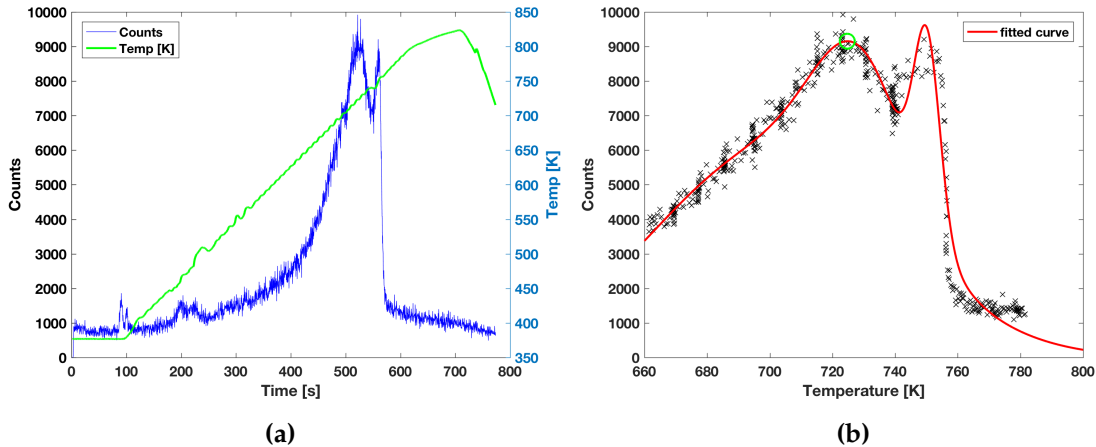


**Figure 4.4:** example of TPD measurements from the new sample. (a) shows data acquired from the quadrupole mass analyser and thermocouple readings. (b) shows the fitted curve to the datapoints within  $\pm 60^\circ\text{C}$  of the estimated peak value.

# 5

# Results

The techniques and procedures presented in the preceding chapter are all used to study an Ir(111) crystal with a graphene monolayer on top.

## 5.1 Graphene on Ir(111)

STM images of pure graphene on Ir(111) are shown in this section. Figure 5.1 shows images of graphene on Ir(111) in different sizes and, Figure 5.1a shows a large image of a graphene monolayer covering the Ir(111) surface. Although the quality of the image is poor, which is seen as lines dragged across the surface, the moiré pattern can be perceived as a pattern of small hexagonal structures. The blurred lines can be caused by the tip picking up an atom which momentarily change the LDOS of the tip, until the atom is dropped on the surface once again. The hexagonal structures, caused by the moiré pattern, are outlined in the top left of the image. Several step edges from the underlying Ir surface are also seen. Several line scans have been performed on these edges, which show that the height difference is  $2\text{\AA} \pm 0.4\text{\AA}$ . This value is consistent with the value of 0.22nm found in the literature. [22,24]

A high resolution image of Graphene on Ir(111) is shown in Figure 5.1b. The moiré pattern is very prominent in this figure, which once again is outlined as the blue hexagon, and the spacing between the individual sites in the moiré unit cell can be determined from a line scan. A line scan was drawn on Figure 5.1b, and two points were positioned in the ATOP sites of the moiré unit cell in order to obtain the moiré periodicity. The moiré periodicity is  $25.2 \pm 0.4\text{\AA}$  according to the literature. [5] This agrees with the length of  $25.24 \pm 1\text{ \AA}$  measured from the line scan, which is seen on Figure 5.1d. Typical defects of the graphene monolayer are seen in this figure, within the blue circle. These are likely to arise from carbon vacancies.

Figure 5.1c shows a high quality image of the graphene monolayer on top of Ir(111). This image is a zoom in of the image shown in Figure 5.1b corresponding to the dashed square. The smaller pattern mentioned before is much more visible in this image. The hexagonal pattern is the graphene monolayer on top of the iridium. The graphene hexagon is sketched as the blue hexagon

and the moiré pattern seen on the two preceding figures is sketched as the dashed blue hexagon. The moiré unit cell is shown in the form of the blue rhombus, where the four dark corners correspond to the ATOP sites. The HCP and FCC sites lie at the corners of the dashed blue hexagon within the outlined moiré unit cell.

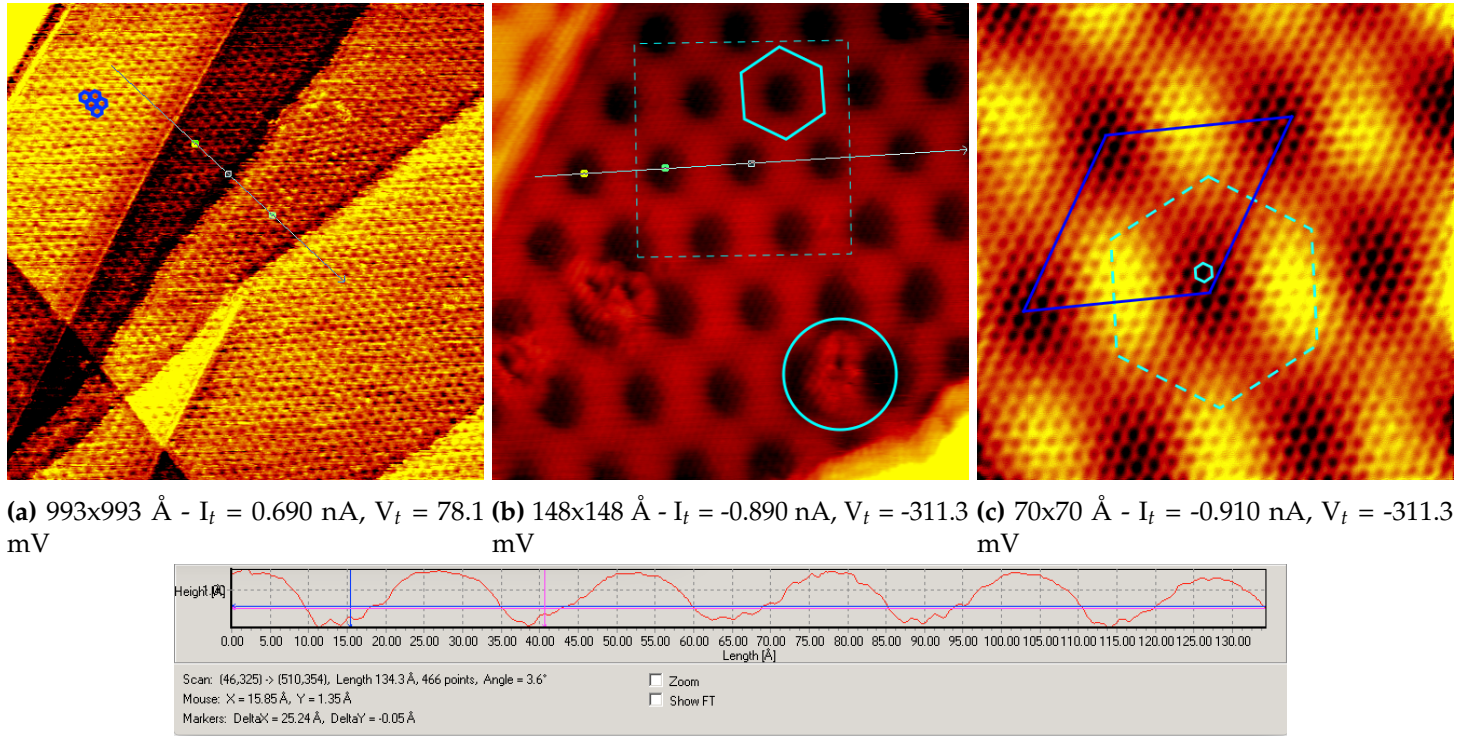


**Figure 5.1:** Clean graphene on Ir(111). (c) is a zoom in of (b) which is shown as the dashed square.

## 5.2 D<sub>2</sub> on Graphene

The following sections present the data from the dose of vibrationally excited molecules. The experiments aimed at determining the threshold temperature of the doser, regarding the hydrogenation of graphene. Hence, the temperature of the doser was varied in order to alter the flux of atoms from the doser, and thereby changing the number of hydrogen recombinations on the walls within the chamber as described in chapter 2. Therefore, the data include dosages at temperatures of 1343°C, 1543°C, and 1745°C. The dosage time and D<sub>2</sub> pressure was identical in all off these doses, in order to ensure that the doser temperature was the only changed variable with an influence on the flux of atomic hydrogen. A dose at 1300°C was also performed. However, the STM broke, and therefore we did not get any images.

### 5.2.1 Full Hydrogen Coverage

A fully hydrogenated surface was used to create STM images. These images were compared to images of the short dosage experiments. The fully hydrogenated surface was made by filling the

chamber with hydrogen at a pirani pressure of  $6.8 \cdot 10^{-2}$ mbar. This pressure should correspond to a chamber pressure of  $5 \cdot 10^{-7}$ mbar, according to the calibration, mentioned in chapter 4. The ion gauge was turned off during the dose, in order to imitate the chamber conditions at short dosage periods. These conditions were left for 12 hours and the sample was scanned afterwards. On figure 5.2 images on different scales can be seen. As seen on figure 5.2a the sample is not just locally hydrogenated. Ring structures are seen covering the surface on this image, instead of the moiré pattern observed on figure 5.1a. These structures are however more clear on the following figure 5.2b, which is a zoom in of figure 5.2a. The most common pattern, of the hydrogenated surface, is ring shaped as structures with a bright rim and a darker center. By comparing figure 5.2b with figure 5.1b it is obvious that the adsorption of hydrogen on the surface changes the LDOS. It is noticeable that the defects on figure 5.1b looks like the ring shaped structures seen on figure 5.2, and hence these defect might be caused by adsorbed hydrogen. Furthermore some H-structures on the saturated surface seem to melt together in a bigger structure, seen as the bone- and three point star shaped structures as pointed out in figure 5.2b. A line scan was performed on the sample in order to check the periodicity of the pattern on the hydrogenated surface. The line scan is seen on figure 5.2c and the related profile is shown in figure 5.2d. The distance between the two points is measured to  $24.2 \pm 1$  Å. This value is very close to the expected periodicity of the moiré unit cell. [22]

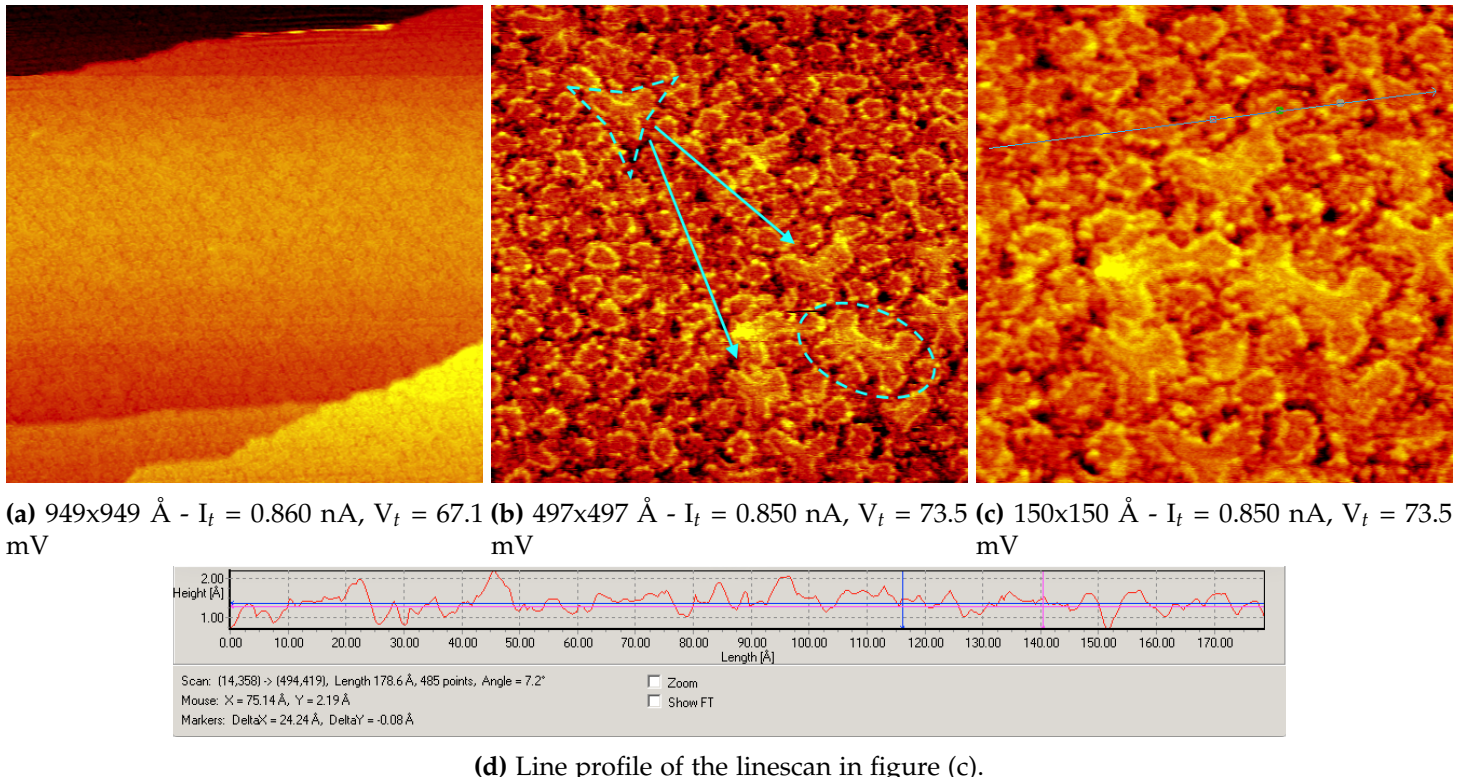


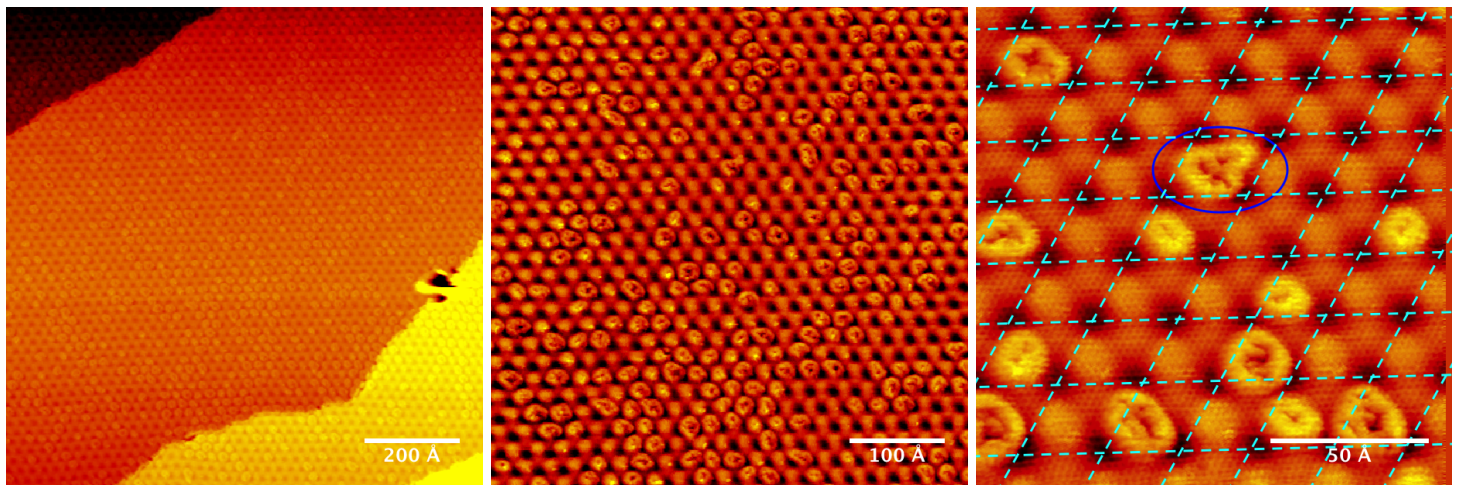
**Figure 5.2:** Fully hydrogenated Gr/Ir(111) surface after 12h D<sub>2</sub> dosage. (c) is a zoom in on (b)

### 5.2.2 1745°C dose

This dosing was performed at a pirani pressure of  $6.8 \cdot 10^{-2}$ mbar, and with the doser set at a temperature of 1745°C. The dosage time was 20 min. The graphene was checked before dosing in order to reduce the number of defects as much as possible. Three images at different scales are shown in Figure 5.3. These images were taken immediately following the completion of the dosing. As seen on figure 5.3a, the surface is far from saturated, compared to figure 5.2a, since the moiré pattern is seen in between areas where the distinct ring structure of the hydrogenation is seen. It is also worth noting that none of the hydrogenated sites melt together to form bigger structures, which indicates that this phenomenon happens as the surface becomes saturated.

In figure 5.3 each moiré unit cell has been sketched out with blue dashed lines. From this it is obvious that hydrogenation only happens at one site in the bottom left corner of the moiré unit cell. Earlier studies suggest that this is the FCC site in the moiré unit cell. [25] It is, however, seen that the hydrogenation expands to the HCP site as well in some of the unit cells, as shown with the dark blue circle.

Individual hydrogen atoms are not distinguishable from the STM images, and therefore the coverage is estimated as a percentage of the number of hydrogenated unit cells to the total number of unit cells. Figures 5.3b and 5.3c were used to calculate an estimate of the hydrogenation of the surface. The coverage on figure 5.3b was calculated to 41% and the coverage on figure 5.3c was calculated to 29%. This means that about one third of the unit cells is hydrogenated after a dosage of excited molecules for 20 min, at a chamber pressure of  $5 \cdot 10^{-7}$ mbar.



(a) 998x998 Å -  $I_t = 1.060$  nA,  $V_t = 67.1$  mV (b) 497x497 Å -  $I_t = 1.080$  nA,  $V_t = 67.1$  mV (c) 150x150 Å -  $I_t = 1.090$  nA,  $V_t = 67.1$  mV

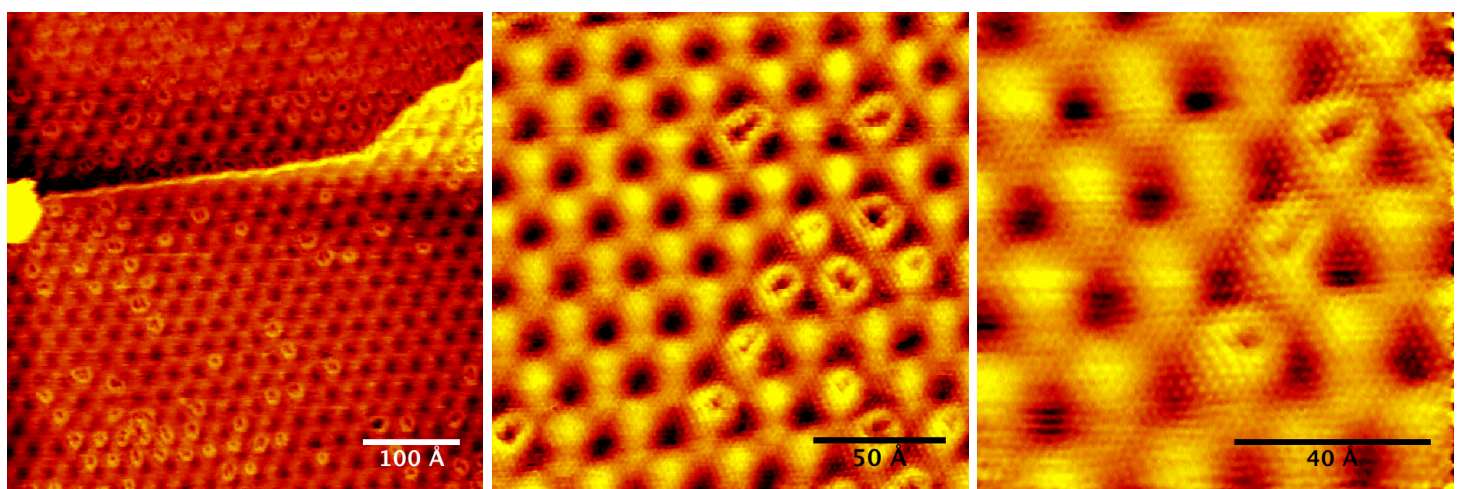
**Figure 5.3:** Hydrogenated Gr/Ir surface after dose of D<sub>2</sub> at a doser temperature of 1745°C.

### 5.2.3 1593°C dose

This dose was performed at a pirani pressure of  $6.8 \cdot 10^{-2}$ mbar and a doser temperature of 1593°C. Again the dose had a duration of 20 min. The images obtained after the dose are shown in figure 5.4. The resemblance between the pictures shown in figure 5.3 and 5.4 is quite high. Again the ring

shaped structures are seen, and the shape of these are very similar to the ones observed earlier. It is seen that several ring structures are seen along the Ir step edge in Figure 5.4b. The energy barrier is known to be less at step edges and dislocations [26], hence molecules excited to lower vibrational states might be able to hydrogenate the graphene in these regions. This could explain the hydrogenation along the step edge.

Figures 5.4a and 5.4b were used to calculate the coverage of hydrogenation, with values of 32% and 25% respectively. These values are however very position dependant, and therefore they do not necessarily reflect the accurate coverage. It is however clear that hydrogenation of the surface has occurred.



(a) 488x488 Å -  $I_t = 0.900$  nA,  $V_t = 190.4$  mV (b) 180x180Å -  $I_t = 1.020$  nA,  $V_t = 190.4$  mV (c) 97x97 Å -  $I_t = 1.020$  nA,  $V_t = 190.4$  mV

**Figure 5.4:** Hydrogenated Gr/Ir surface after dose of D<sub>2</sub> at a doser temperature of 1593°C.

#### 5.2.4 1343°C dose

The pirani pressure was measured to  $6.8 \cdot 10^{-2}$  mbar, and the doser had a temperature of 1343°C during this dose. Hydrogen was dosed for 20 min as earlier. As seen on figure 5.5 several high quality pictures of the sample was taken. On figure 5.5a it would seem like some hydrogen is adsorbed due to the observation of several ring shaped structures. As a smaller image is taken such as the one in figure 5.5b the defects looks somewhat different from those seen earlier on figures 5.4b and 5.3c. The ring shaped structures are much smaller in diameter on figure 5.5b, even though the scanning parameters are close to each other.

A high resolution image is seen on figure 5.5c, where the hexagonal graphene is highly visible. On this picture it is clear that the graphene is defected, although it is unclear whether this is due to the presence of hydrogen. It is also seen that the shape of the sites in the moiré unit cell looks different than earlier although both pictures are from the same scan session. This is due to a tip effect, where the LDOS of the tip probably has changed, which has an influence on the tunnelling current. This might happen if the tip picks up an atom from the surface, or if the physical dimensions of the tip changes after a tip treatment.

It should be noted that the graphene had defects before the dose was initiated. The abundance of these defects was indistinguishable, when comparing before and after the dose. Therefore it is not possible to conclude whether the threshold temperature of the hydrogen adsorption from excited molecules lies at 1340°C. It is however very likely that no hydrogen is adsorbed. In order to investigate the threshold temperature further, it would be rational to conduct TPD measurements of the sample after hydrogen dosage at 1343 °C.

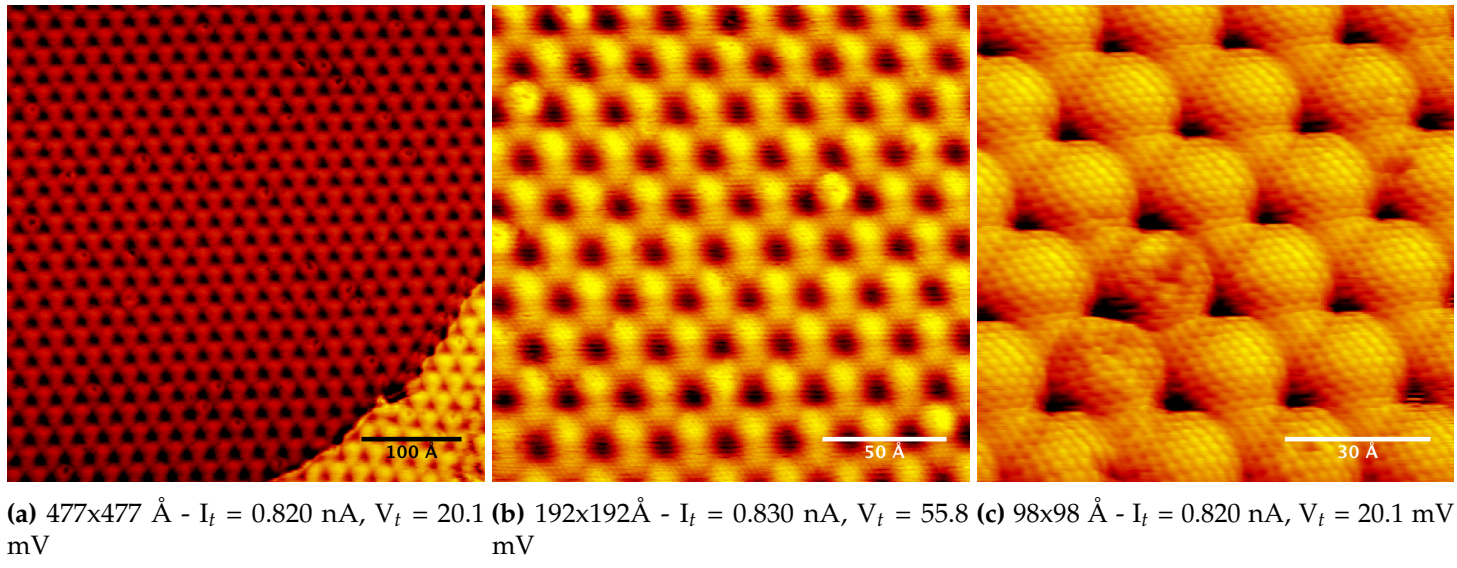


**Figure 5.5:** Hydrogenated Gr/Ir surface after dose of D<sub>2</sub> at a doser temperature of 1343°C.

## 5.3 TPD measurements

In the following sections, TPD measurements from graphene on Ir(111) exposed to both hot molecules and atoms are compared.

### 5.3.1 Atomic and molecular D2 - single layered sample

In figure 5.8 below, the data from the TPD is gathered in two different figures. TPD measurements were made following doses of both vibrationally excited molecules and atoms on the new sample with a fresh monolayer of graphene on Ir(111). Figure 5.8b shows the TPD data following a 60 min dose of D<sub>2</sub> at a chamber pressure of  $5 \cdot 10^{-7} \text{ mbar}$  and a doser temperature of 1740°C. Figure 5.6b shows the data following a 60 min dose of hydrogen atoms at a chamber pressure of  $5 \cdot 10^{-7} \text{ mbar}$  and a doser temperature of 1740°C.

After dosage of excited molecules a single peak is observed which is seen in Figure 5.8b. A big peak is seen after the main peak, at a temperature of about 800K. This is due to a temperature spike caused by the Eurotherm temperature controller, which was poorly calibrated as explained in chapter 4. Noticeable fluctuations, caused by this problem, are also seen in Figure 5.6b. This dataset was gathered during the same chamber and sample conditions as the blue graph in Figure 5.8b.

Sample	fig.5.8b blue	fig.5.8a green	fig.5.6b blue	fig.5.8b green	fig.5.7 green	fig.5.7 red
Peak T [K]	724.8	698.4	694.0	709.1	739.1	753.4
$E_{des}^{Redhead}$ [eV]	2.1±0.4	2.0±0.4	2.0±0.4	2.0±0.4	2.1±0.4	2.1±0.4

Table 5.1

The temperature at the peak was found by the procedure described in chapter 4. The single peak in figure 5.8b must correspond to the hydrogen adsorbed on the HCP and FCC sites in the moiré unit cell. This statement is supported by the preceding STM pictures that show no sign of hydrogen dimers in the ATOP sites. The temperature of this peak was found for 6 datasets in all, and the values of these are shown in table 5.1. The calculated energies of desorption by the Redhead method are all around 2 eV. This value is close to the calculated average hydrogen binding energy of 2.20 eV [27] within a graphane like island. Further calculations of the adsorption barrier is made in recent research. Here it is found that the initial hydrogen molecule perceives an adsorption barrier of 3eV. Hereafter the adsorption barrier undergoes a reduction of 1 eV due to the distortion of the graphene from the  $sp^2$  to  $sp^3$  rehybridization.

Another peak appears when observing the graphene on Ir(111) sample after it has been dosed with hot atoms as seen in Figure 5.6b. Hydrogen desorbs from the sample at two different desorption energies, which is seen from the two peaks. The temperature of these peaks were found by the same procedures as earlier, and the values were found to be 550.4K and 694.0K. The lower peak suggests that a different type of Gr-H bond is present. The most plausible explanation is the presence of hydrogen dimers on the ATOP site of the moiré unit cell which has been found by DFT calculations. [27] Earlier TPD measurements of deuterium dosed on highly ordered pyrolytic graphite (HOPG) have shown that dimer peaks appear at 445K and 560K. [28] These values are in correspondence with the peak in Figure 5.6b. However, through discussions with the lab supervisor it was suggested that the peak intensity in this figure is too high to only stem from dimers. Therefore hydrogen must desorb from another source within the chamber under the TPD measurements. It is reasonable that this contribution come from the desorption of hydrogen from the Tantalum sample holder.

## 5.4 Graphene bilayered sample

As a further study of the adsorption of hydrogen on Gr/Ir, patches of graphene bilayers were grown on the sample by annealing in ethylene for a long period of time. The sample was investigated with several techniques, and the results are presented in the following sections.

### 5.4.1 TPD of bilayered sample

TPD measurements were conducted on the sample before and after the long anneal. The red graph in figure 5.7 is the TPD results following a 60 min dose of  $D_2$  at a chamber pressure of  $1.04 \cdot 10^{-6}$ mbar and with a doser temperature of 1740°C.

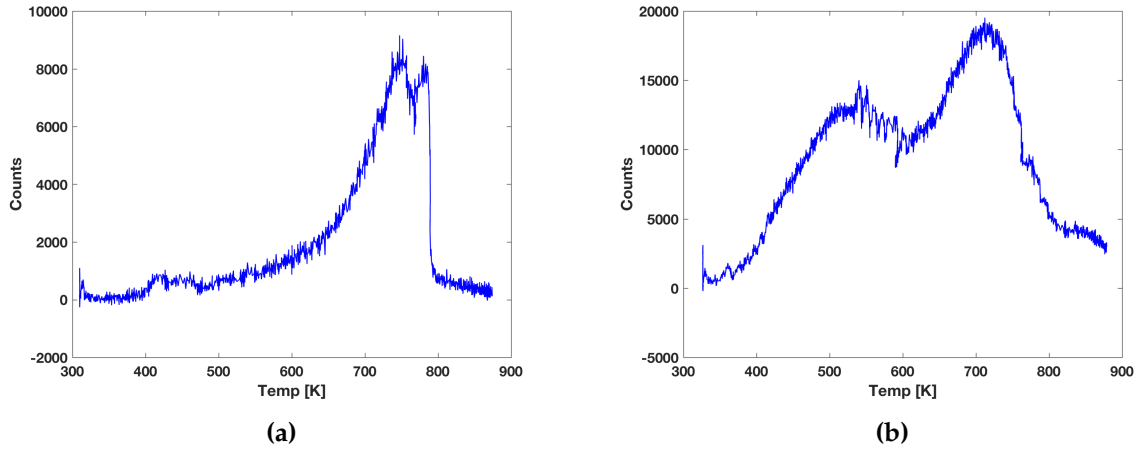


**Figure 5.6:** TPD measurements following doses of  $D_2$  and hot atoms. (a) shows the graph following a 1 hour  $D_2$  dose on graphene on Ir(111) with a doser temperature of 1740 °C and a chamber pressure of  $5 \cdot 10^{-7}$ mbar. and (b) shows the graph following a 1 hour  $D$  dose on graphene on Ir(111) with a doser temperature of 1740 °C and a chamber pressure of  $5 \cdot 10^{-7}$ mbar.

The green graph corresponds to the sample after bilayers supposedly were grown. Bilayers were grown by exposing the sample to ethylene at a pressure of  $1 \cdot 10^{-6}$ mbar for 60 min, while the sample was heated to 990°C. The sample was dosed with atomic hydrogen at a chamber pressure of  $1.04 \cdot 10^{-6}$ mbar and with a doser temperature of 1740K as well as before. It is seen that the peak value this time is around 6.000, which means that the increased amount of bilayers reduce the amount of hydrogen on the surface by a significant amount. This suggests that hydrogen is not adsorbed on the bilayered graphene. This theory is supported by the STM pictures below. It should be noted that only two datasets were gathered from this experiment. The peak intensity from the TPD measurements tends to vary slightly and hence the amount of bilayers grown on the sample might not be perfectly related to the drop in peak intensity.

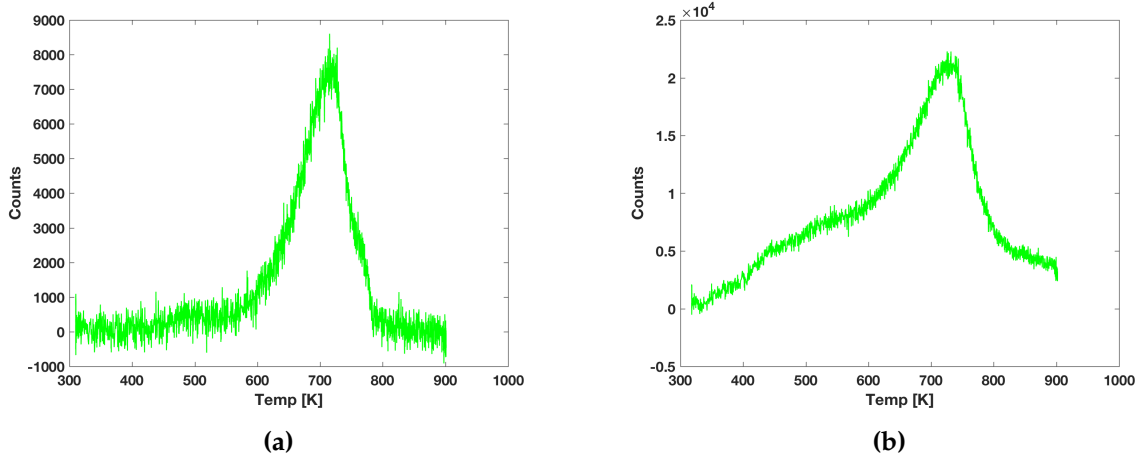


**Figure 5.8:** TPD measurements following doses of D<sub>2</sub> and hot atoms. (a) shows the graph following a 1 hour D<sub>2</sub> dose on graphene on Ir(111) with a doser temperature of 1740 °C and a chamber pressure of  $5 \cdot 10^{-7}$  mbar. and (b) shows the graph following a 1 hour D dose on graphene on Ir(111) with a doser temperature of 1740 °C and a chamber pressure of  $5 \cdot 10^{-7}$  mbar.

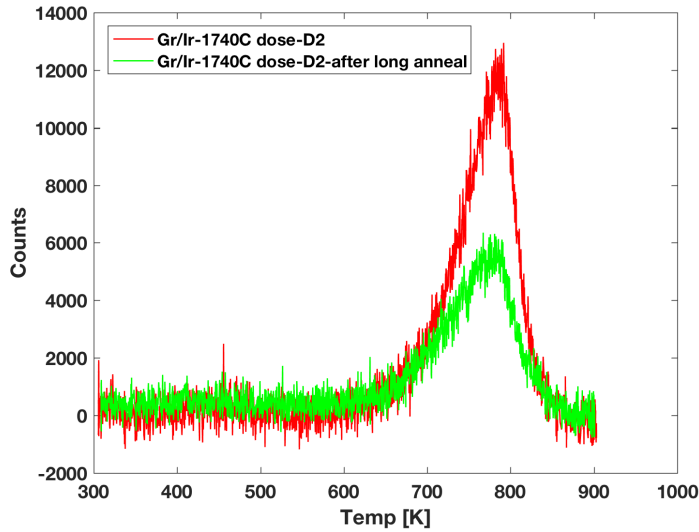


**Figure 5.7:** TPD measurements after doses of D<sub>2</sub> at a pressure of  $1.04 \cdot 10^{-6}$  and a doser T of 1740°C. The red graph is prior to a 60 min growth of bilayers where the 990°C hot sample was exposed to ethylene for 60 min at a pressure of  $1 \cdot 10^{-6}$  mbar

#### 5.4.2 STM images of bilayers

In the following section STM images of bilayer patches are included. These images are made prior to the long anneal, and are therefore not directly related to the experiment mentioned in the preceding section. It was not possible to make images of the sample after the long anneal in ethylene, since the STM was broken. Bilayers were however present on the surface prior to the

long anneal, and the following images show some of the key points about these.

The images in figure ?? are made after the 12 hour dose of hydrogen at a chamber pressure of  $1 \cdot 10^{-5}$  mbar with the ion gauge turned on. Hence the surface is fully hydrogenated which is somehow different to see due to the large images. On figure 5.9a, the three-point-star-structures characteristic for the hydrogenated surface are however seen, which is pointed out with the blue arrows. Bilayer patches are seen on the top half of the figure, and none of the structures characteristic for the fully hydrogenated surface are seen. A new superstructure is however seen with the individual flower-like structures, with a center circle surrounded by six other circles, construct a bigger pattern.

On figure 5.9b a linescan was made across the edge of the graphene monolayer-bilayer edge. The corresponding line profile is shown in figure 5.9d, and from this the height difference is measured to  $2.97 \pm 0.5$  Å. The bilayer edge is therefore significantly higher than the Iridium step edge, and much closer to the layer height of HOPG which is 0.35nm. [29]

In order to investigate the bilayer superstructure further, a zoom in of figure 5.9b was made as seen in figure 5.9c. The graphene sheet is seen due to the atomic resolution, and it is obvious that no hydrogen is adsorbed to the surface. This is consistent with the data from the TPD measurements. Furthermore it is seen that the consistency in the superstructure is absent. Some areas of the bilayer has a cluster of three circles forming a triangle that points either up or down. These are highlighted in the left side of the picture. Other areas seem to have the flower-like structure mentioned earlier, but with an overlapping hexagon. An attempt to determine the periodicity of the superstructure was done by doing a linescan between two identical parts of the pattern. As seen on figure 5.9c the linescan was drawn between two down facing triangles, and the distance between these were measured from the bottom corner. The line profile is shown in figure 5.9e and the length between the points is measured to  $45.78 \pm 1$  Å.

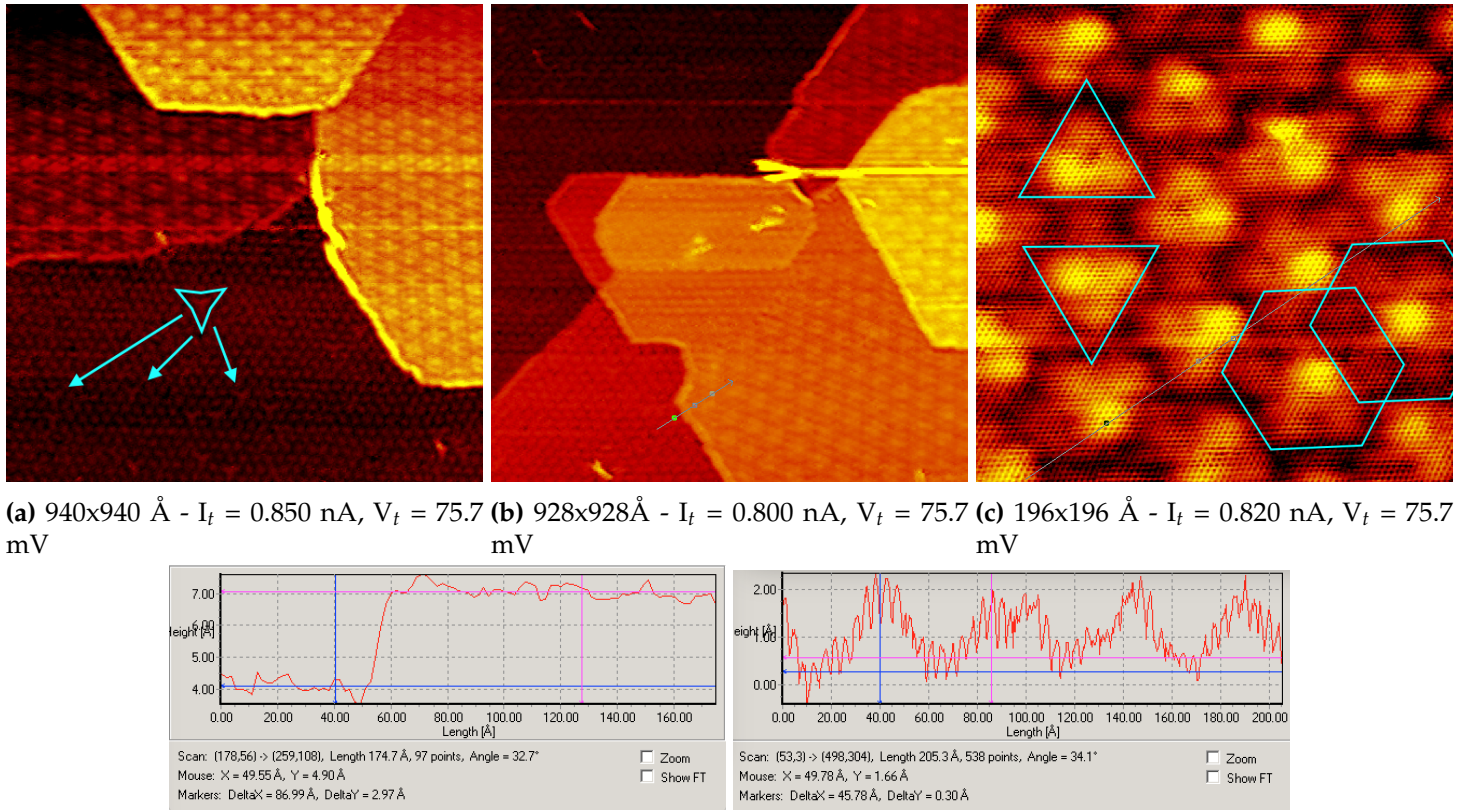


Figure 5.9: Patches of bilayered graphene on Ir after a hydrogen dose at  $1 \cdot 10^{-5}$  mbar for 12h.

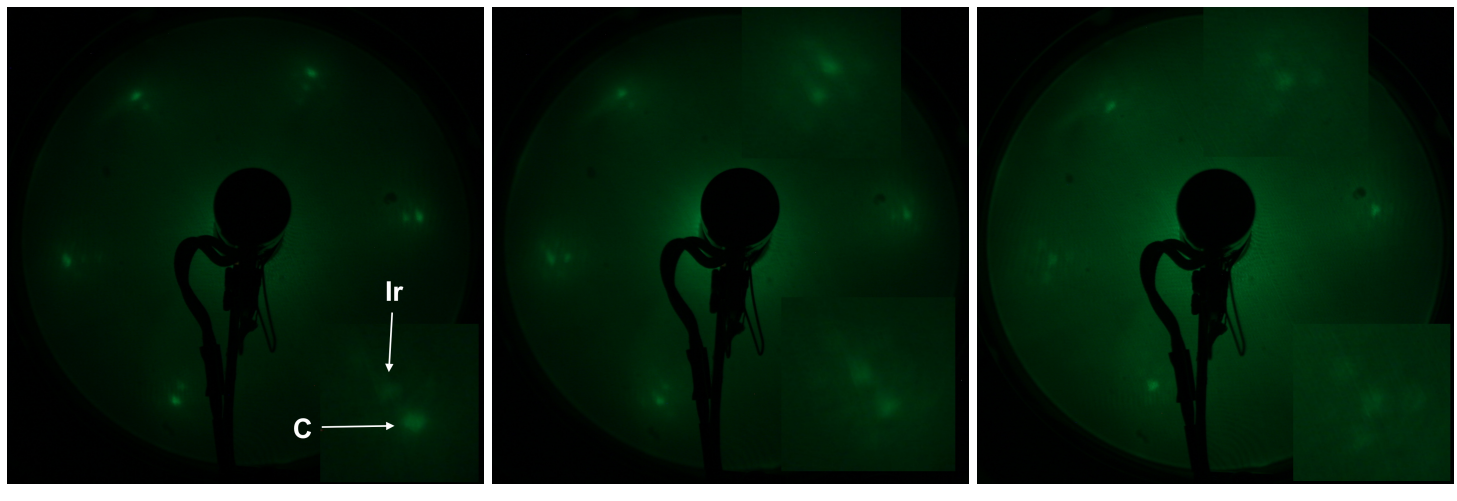
### 5.4.3 LEED of bilayered sample

LEED was performed on the sample after an ethylene anneal with a chamber pressure of  $7 \cdot 10^{-7}$  mbar. The figures in 5.10 show pictures of the fluorescent screen within the UHV chamber from which the LEED was performed. The image on figure 5.10a shows the fluorescent screen after the untreated sample was exposed to an electron beam with an energy of 145eV. The spots marked out with the marked arrows show the diffraction pattern from the underlying Ir(111) surface, as well as the graphene sheet on top of the surface. [5]

The sample was then flashed to a low temperature in order to maintain any bilayers, and the sample was once again exposed to an electron beam of energy 145eV. The top and bottom right corner of the hexagonal pattern is enlarged in figure 5.10b. From this figure it is clear that some extra spots appear around the Ir and C spots pointed out in the previous figure. These spots arise from the moiré pattern of the graphene on Ir(111) surface. The reason why these spots were absent in the previous figure might be caused by a high amount of contaminants on the surface. These ruin the periodicity of the surface, and hence also the electron scattering, which then becomes smeared out. After annealing to a low temperature these contaminants should be gone, leaving the surface clean with small patches of bilayered graphene. The patches of bilayered graphene should however also cause a different scattering due to the changed periodicity as seen in figure 5.9c. If figure 5.10b and 5.10c is compared it does look like the spot belonging to the carbon atoms

#### 5.4. Graphene bilayered sample

and the surrounding moiré spots in figure 5.10b are less distinct. These results might therefore indicate that bilayers are present on the surface in figure 5.10b and to a lesser extent in figure 5.10c. Since the picture in figure 5.10c is taken prior to an 1090°C anneal, it is reasonable to conclude that the bilayer patches desorb from the surface when annealing to this temperature.[Reference til desorption af bilayers?]



(a) LEED without flashing. 145eV. (b) LEED after low T flash. 145eV (c) LEED after 1090°C flash. 145eV

**Figure 5.10:** LEED pictures from the Gr/Ir sample with bilayers. [Reference til Antonija/Hoffman-lab]

# 6

## Conclusion and future perspectives

### 6.1 conclusion and future perspectives

A

## Additional figures

# Bibliography

- [1] K. S. Novoselov, V. I. Fal[prime]ko, L. Colombo, P. R. Gellert, M. G. Schwab, and K. Kim. A roadmap for graphene. *Nature*, 490(7419):192–200, 10 2012.
- [2] L. Solymar and D. Walsh. *Electrical properties of materials, EIGHTH EDITION*. OXFORD UNIVERSITY PRESS, 2010.
- [3] A. H. Castro Neto, F. Guinea, N. M. R. Peres, K. S. Novoselov, and A. K. Geim. The electronic properties of graphene. *Rev. Mod. Phys.*, 81:109–162, Jan 2009.
- [4] Ludwig A Kibler. Preparation and characterization of noble metal single crystal electrode surfaces. *Short Course Held at the 51st and 53rd Annual Mtg of the ISE*, 2003.
- [5] Alpha T N'Diaye, Johann Coraux, Tim N Plasa, Carsten Busse, and Thomas Michely. Structure of epitaxial graphene on ir(111). *New Journal of Physics*, 10(4):043033, 2008.
- [6] Line Kyhl. Figures made by line kyhl.
- [7] Richard Balog, Bjarke Jørgensen, Louis Nilsson, Mie Andersen, Emile Rienks, Marco Bianchi, Mattia Fanetti, Erik Laegsgaard, Alessandro Baraldi, Silvano Lizzit, Zeljko Sljivancanin, Flemming Besenbacher, Bjørk Hammer, Thomas G Pedersen, Philip Hofmann, and Liv Hornekaer. Bandgap opening in graphene induced by patterned hydrogen adsorption. *Nature Materials*, 9(4):315–319, 4 2010.
- [8] Line Kyhl, Richard Balog, Thierry Angot, Liv Hornekær, and Régis Bisson. Hydrogenated graphene on ir(111): A high-resolution electron energy loss spectroscopy study of the vibrational spectrum. *Phys. Rev. B*, 93:115403, Mar 2016.
- [9] R. I. Hall, I. Čadež, M. Landau, F. Pichou, and C. Schermann. Vibrational excitation of hydrogen via recombinative desorption of atomic hydrogen gas on a metal surface. *Phys. Rev. Lett.*, 60:337–340, Jan 1988.
- [10] Y. Miura, H. Kasai, W. Diño, H. Nakanishi, and T. Sugimoto. First principles studies for the dissociative adsorption of h<sub>2</sub> on graphene. *Journal of Applied Physics*, 93(6), 2003.
- [11] P. J. Eenshuistra, J. H. M. Bonnie, J. Los, and H. J. Hopman. Observation of exceptionally high vibrational excitation of hydrogen molecules formed by wall recombination. *Phys. Rev. Lett.*, 60:341–344, Jan 1988.

- [12] The aarhus stm. <http://inano.au.dk/research/research-platforms/nanoanalysis/scanning-tunneling-microscopy/>. Accessed: 2016-06.
- [13] Gerd Binnig and Heinrich Rohrer. Scanning tunneling microscopy—from birth to adolescence. *Rev. Mod. Phys.*, 59:615–625, Jul 1987.
- [14] DAWN BONNELL. *Scanning Probe Microscopy and Spectroscopy: Theory, Techniques, and Applications, 2nd Edition*. WILEY-VCH, 2001.
- [15] G. Binnig, H. Rohrer, Ch. Gerber, and E. Weibel. Surface studies by scanning tunneling microscopy. *Phys. Rev. Lett.*, 49:57–61, Jul 1982.
- [16] W.A. Steele, G. Zgrablich, and W. Rudzinski. *Volume 104. Equilibria and Dynamics of Gas Adsorption on Heterogeneous Solid Surfaces*. Elsevier Science, 1996.
- [17] Desorption lecture slides. [http://th.fhi-berlin.mpg.de/th/lectures/summer\\_term\\_2006/6\\_desorption.pdf](http://th.fhi-berlin.mpg.de/th/lectures/summer_term_2006/6_desorption.pdf). Accessed: 2016-06.
- [18] Sven L.M. Schroeder and Michael Gottfried. Temperature-programmed desorption (tpd) thermal desorption spectroscopy (tds), 2002.
- [19] Thermal analysis - tds. [http://www.fhi-berlin.mpg.de/acnew/department/pages/teaching/pages/teaching\\_\\_wintersemester\\_\\_2005\\_2006/ranke\\_tds\\_251105.pdf](http://www.fhi-berlin.mpg.de/acnew/department/pages/teaching/pages/teaching__wintersemester__2005_2006/ranke_tds_251105.pdf). Accessed: 2016-06.
- [20] Surface chemistry. <http://www.chemistryexplained.com/St-Te/Surface-Chemistry.html>. Accessed: 2016-06.
- [21] Hydrogen atom beam source - datasheet. <http://www.mbe-komponenten.de/products/pdf/data-sheet-habs.pdf>. Accessed: 2016-06.
- [22] Johann Coraux, Alpha T N'Diaye, Martin Engler, Carsten Busse, Dirk Wall, Niemma Buckanie, Frank-J Meyer zu Heringdorf, Raoul van Gastel, Bene Poelsema, and Thomas Michely. Growth of graphene on ir(111). *New Journal of Physics*, 11(2):023006, 2009.
- [23] Pyrometer handbook. Work of IMPAC Infrared GmbH. 2004.
- [24] Johann Coraux, Alpha T N'Diaye, Carsten Busse, and Thomas Michely. Structural coherency of graphene on ir (111). *Nano letters*, 8(2):565–570, 2008.
- [25] Jakob Jørgensen, Antonija Grubisic Cabo, Line Kyhl Hansen, Richard Balog, Philip Hofmann, and Liv Hornekær. Unpublished.
- [26] Line Kyhl, Régis Bisson, Richard Balog, Michael Groves, Andrew Cassidy, Jill Miwa, Jakob Jørgensen, Antonija Grubisic Cabo, Susanne Halkjær, Jan Knudsen, Samuli Urpelainen, Hendrik Bluhm, Thierry Angot, Philip Hofmann, Bjørk Hammer, and Liv Hornekær. Unpublished.

- [27] Richard Balog, Mie Andersen, Bjarke Jørgensen, Zeljko Sljivancanin, Bjørk Hammer, Alessandro Baraldi, Rosanna Larciprete, Philip Hofmann, Liv Hornekær, and Silvano Lizzit. Controlling hydrogenation of graphene on ir (111). *ACS nano*, 7(5):3823–3832, 2013.
- [28] Liv Hornekær, Ž Šljivančanin, W Xu, R Otero, E Rauls, Ivan Stensgaard, Erik Lægsgaard, Bjørk Hammer, and Flemming Besenbacher. Metastable structures and recombination pathways for atomic hydrogen on the graphite (0001) surface. *Physical review letters*, 96(15):156104, 2006.
- [29] J. Červenka and C. F. J. Flipse. Structural and electronic properties of grain boundaries in graphite: Planes of periodically distributed point defects. *Phys. Rev. B*, 79:195429, May 2009.
- [30] J. Tersoff and D. R. Hamann. Theory and application for the scanning tunneling microscope. *Phys. Rev. Lett.*, 50:1998–2001, Jun 1983.